

Characterization of single layer anti-reflective coatings for bolometer-based rare event searches

E.V. Hansen^a, N. DePorzio^b, & L. Winslow^c

^a*Drexel University, Department of Physics, Disque Hall Rm 816 32 South 32nd Street, Philadelphia, PA 19104*

^b*Northeastern University, Department of Physics, 360 Huntington Ave., 111 Dana Research Center, Boston, MA 02115, USA*

^c*Massachusetts Institute of Technology, Department of Physics, 77 Massachusetts Avenue, Cambridge, MA 02139, USA*

E-mail: ^aevh32@drexel.edu, ^clwinslow@mit.edu

ABSTRACT: Combining analysis from phonon signals and photon signals is a powerful technique for reducing backgrounds in bolometer-based rare event searches. Anti-reflective coatings can significantly increase the performance of the secondary light-sensing bolometer in these experiments. As a first step toward these improvements, coatings of SiO₂, HfO₂, and TiO₂ on Ge and Si wafers were fabricated and characterized at room temperature and multiple angles of incidence.

KEYWORDS: radiation detector, scintillating bolometers, double beta decay, antireflective coatings.

Contents

1. Introduction	1
2. Light Emission and Simulation	2
3. Anti-Reflective Coatings	2
3.1 Comparison to Previous Experiment (<i>Mancuso, Beeman, et.al.</i>)	4
3.2 Choice of Substrates	4
3.3 Choice of Coatings	5
4. Other Requirements	6
5. Fabrication	7
6. Characterization	8
7. Predicted Reflectance	10
8. Conclusion	12

1. Introduction

Rare-event searches are being pursued to answer some of the greatest mysteries in physics at the present time, namely: the nature of dark matter through direct detection (DM) and the possible Majorana nature of the neutrino through searches for neutrinoless double-beta decay ($0\nu\beta\beta$). In these experiments, combining multiple signals is a powerful active background rejection technique. Scintillating bolometers use the combination of phonon and photon signals to discriminate between particle types. The CUPID (CUORE with Upgraded Particle IDentification) [1] and CRESST [2, 3] detectors are pursuing this technology for $0\nu\beta\beta$ and DM searches respectively.

A scintillating bolometer measures a phonon signal: the change in temperature in a crystal due to the interaction of charged particles with the crystal lattice. These interactions also produce a photon signal: scintillation light which is detected by a target Ge or Si bolometer. An anti-reflective coating on the target bolometer, as shown in Figure 1, increases light collection and therefore improves the energy resolution of the light measurement. In this paper, we discuss the optimization of an anti-reflective coating for two promising scintillating crystals containing $0\nu\beta\beta$ isotope: ZnSe and ZnMoO₄. We also discuss optimizing the anti-reflective coating to detect Cherenkov light in non-scintillating crystals like TeO₂, the current CUORE crystal.

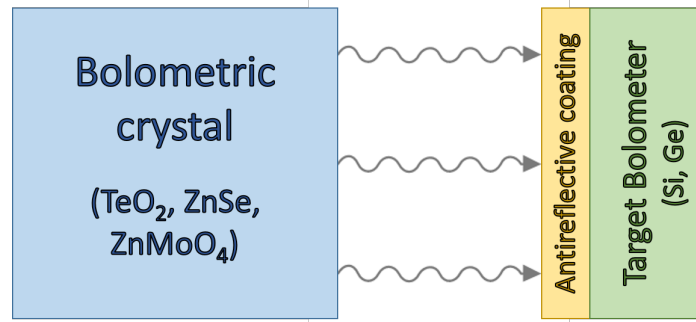


Figure 1. An anti-reflective coating is deposited onto the auxiliary bolometer to improve transmission of Cherenkov or scintillation photons from the bolometric crystal.

2. Light Emission and Simulation

The scintillation spectra of ZnSe and ZnMoO₄ are well characterized at temperatures down to 8 K. The spectra peak at 645 nm and 610 nm respectively [4]. The absorption cutoff for TeO₂ is 350 nm [5], forming the effective peak of the Cherenkov spectrum. Our default target bolometer is composed of hyper-pure germanium (HPGe) thin slabs run at a standard operating temperature of 15-20 mK. We also study silicon (Si) since it has equivalent performance at these operating temperatures and is widely available. Using refractive index data from [6], we find Ge substrates reflect ~50% of normal incident light while Si substrates reflect ~35%; see Figure 2. The results for ZnSe scintillation at 645 nm and TeO₂ Cherenkov light are similar.

As shown in Figure 2, the angle of incidence is critical for understanding the response of the target bolometer. A GEANT4[7–9] Monte Carlo was constructed to examine the incidence angles of photons produced from beta particles distributed isotropically in position, angle, and energy throughout a ZnMoO₄ bolometer. The light produced from these events was allowed to scatter within the crystal until it attenuated, escaped, or struck a target bolometer 1mm away from a single face. The relevant physical and optical properties of these materials, if not specifically included in the Geant4 NIST database, were obtained from literature[10–12]. Results are shown in Figure 3. The average angle of incidence was 32° with a standard deviation of 21°. This is a sizable deviation from normal incidence, and must be considered when selecting a coating/bolometer combination. In future work, the results of these measurements for the final target bolometers can be used either as input to or a benchmark of the Monte Carlo.

3. Anti-Reflective Coatings

As seen in Figure 1, the target bolometer can be supplemented by depositing an anti-reflective coating to create a thin film structure where layers of contrasting refractive indices produce destructive interference in reflected beams and constructive interference in transmitted beams. This results in an overall increase of transmission. The performance of this structure depends heavily on the light's incident angle, wavelength, and polarization. The reflection coefficient for unpolarized light

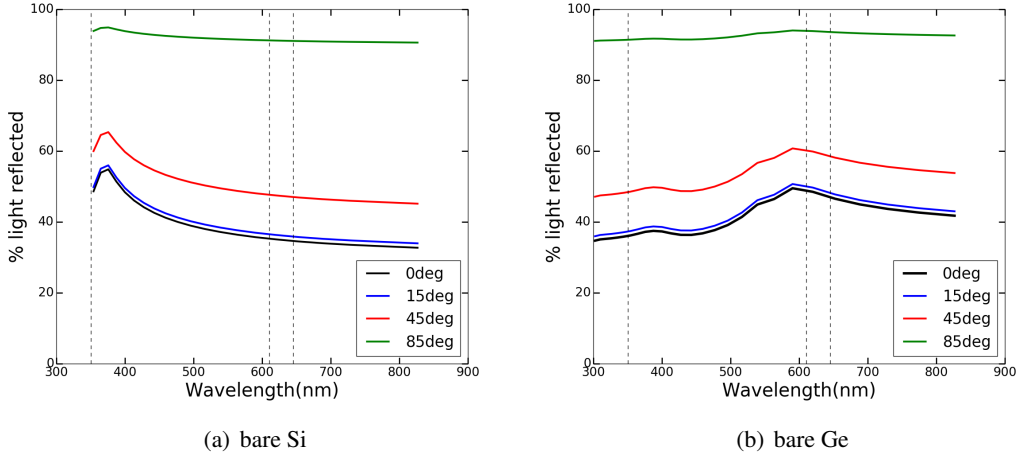


Figure 2. Reflectivity of light of various angles of incidence on bare substrates: (a) Si and (b) Ge [6]. Vertical dashed lines indicate the cutoff wavelength of TeO₂ (350 nm) and the peak wavelengths of scintillation for ZnMoO₄ (610 nm) and ZnSe (645 nm). For these wavelengths and normal incidence, bare Si reflects over 30% of incoming light; bare Ge reflects over 40%.

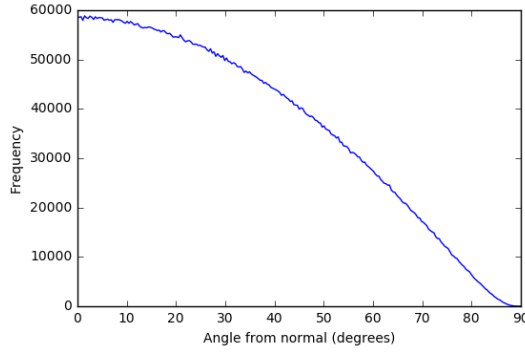


Figure 3. Results of a GEANT4 Monte Carlo to measure the angle of incidence of photons generated by beta particles from a TeO₂ bolometer. The angle of incidence is plotted with respect to normal incidence (0). This clearly demonstrates the failure of a normal incidence assumption.

incident on a single layer anti-reflective coating (SLAR) is written [13] as:

$$R = \frac{1}{2}(|r_s|^2 + |r_p|^2) \quad (3.1)$$

$$r_s = \frac{r_{01,s} + r_{12,s} \exp(-2i\beta)}{1 + r_{01,s} r_{12,s} \exp(-2i\beta)} \quad r_p = \frac{r_{01,p} + r_{12,p} \exp(-2i\beta)}{1 + r_{01,p} r_{12,p} \exp(-2i\beta)} \quad (3.2)$$

where the subscripts *s* and *p* refer to waves parallel or perpendicular to the plane of incidence and the numerical subscripts refer to the medium in which the light is traveling: 0 for the outside medium (ideally vacuum), 1 for the SLAR, and 2 for the substrate. If θ_{inc} is the angle of incidence onto the SLAR of thickness *d*, the phase shift is given by $\beta = 2\pi d N \cos \theta_{\text{inc}} / \lambda$. The individual

reflection coefficients are given by

$$r_{jm,s} = \frac{N_m \cos \theta_j - N_j \cos \theta_m}{N_m \cos \theta_j + N_j \cos \theta_m} \quad r_{jm,p} = \frac{N_j \cos \theta_j - N_m \cos \theta_m}{N_m \cos \theta_j + N_j \cos \theta_m} \quad (3.3)$$

and

$$N_j = (n_j + ik_j) \quad \theta_j = \arcsin \left(\frac{N_0}{N_j} \sin \theta_{\text{inc}} \right) \quad (3.4)$$

where n and k are the real and imaginary parts, respectively, of the complex refractive index of the material and are also dependent on wavelength. The ideal coating will minimize R with respect to n and k .

3.1 Comparison to Previous Experiment (*Mancuso, Beeman, et.al.*)

This work builds upon the study done by Mancuso et al. [17]. They tested SiO₂ films, 70 nm thick and deposited on a Ge substrate using a sputtering technique. The films were evaluated at ~ 10 mK. SiO₂ decreased reflectivity by 18-20% [17]. In this paper, we manufacture similar coatings but characterize them at room temperature so that we can study the angular effects.

In Mancuso et.al., the scintillation light is assumed to reach the target bolometer at normal incidence. As we show in Section 2 and as they indicate in their paper, this is a crude assumption. From first principles, the refractive index in the crystals of interest, ZnSe, ZnMoO₄, and TeO₂, is high enough to allow total internal reflection at a relatively low angle; see Table 1. This implies that even a slight deviation from normal (in the plane of incidence) as the ray leaves the primary bolometer can cause the refracted ray to deviate significantly from normal as it strikes the target bolometer. The distance between primary and target bolometers is small enough (≤ 1 cm) that the angle of incidence on the target bolometer will range from 0° to roughly 88° in the plane of incidence (assuming a CUORE-sized 5cm \times 5cm crystal). From Equations 3.1-3.4, it is clear that a phase difference between reflected waves from the film layer and reflected waves from the substrate layer is introduced whenever the incident angle is non-normal, leading to a substantial change in reflectivity for non-normal incidence.

3.2 Choice of Substrates

Ge is the logical choice for the target bolometer because it absorbs photons better than Si in the visible range; the absorption coefficient of Ge is roughly two orders of magnitude greater [18]. However, Si is more readily available and the manufacturing processes are extremely well understood.

Table 1. Refractive index and total internal reflection angles for bolometer materials. At or above this angle from normal to the surface, a photon cannot exit the crystal into the vacuum. The asterisk indicates that few data points exist for λ in the ROI.

Material	$n(\lambda)$	θ_{crit}
ZnSe	2.58 (645 nm) [14]	22.8°
ZnMoO ₄	~ 1.90 (655 nm)* [15]	31.7°
TeO ₂	2.25 (645 nm) [16]	26.4°

Table 2. refractive index at 645nm for coatings considered in this work.

Material	n (645nm)	Source
Al ₂ O ₃	1.76	Malitson (1972) [22]
HfO ₂	2.10	Wood (1990) [23]
Si ₃ N ₄	2.00	Philipp (1973) [24]
SiO ₂	1.48	Gao (2013) [25]
TiO ₂	2.58	Devore (1951) [26]

These include techniques that could improve anti-reflective coatings, such as micromachining and deposition masking [19]. Finally, Ge has a specific heat ~ 4.5 times greater than that of Si [20]. Because signal amplitude is inversely proportional to the heat capacity of the device, Si detectors can be made into much larger systems without sacrificing signal quality [21]. Considering these factors, we chose to study both Ge and Si as target bolometer candidates for this work.

3.3 Choice of Coatings

For a particular substrate, the minimum possible reflectivity using a SLAR can be calculated using the curves from Equation 3.1. For a Ge substrate and incident 645 nm light from the ZnSe scintillation peak, the complex refractive index of Ge has components $n = 5.36$ and $k = 0.705$. Assuming no losses to the thin film and normal incidence, the reflection coefficient can be decreased maximally with a coating medium with refractive index $n = 2.32$. The closest match considering available materials is TiO₂; see Table 2. HfO₂ is also a possibility. Performing the same calculation for a Si substrate, the minimum reflectivity is achieved for a coating with $n = 1.96$. Si₃N₄, HfO₂, and Al₂O₃ (sapphire) are good matches.

A second anti-reflective layer can be used to further reduce reflectivity. The optimization proceeds similarly to above, except that, in this case, the refractive index is tuned to the first coating instead of the substrate. For example, a Ge-TiO₂ target system could be improved by adding second coating with a refractive index of $n = 1.52$. GeO₂ ($n = 1.60$ [27]) is not readily available, but the more common SiO₂ is a good candidate. Traditionally, SiO₂ has been used as a single layer coating for Si substrates because it is readily available, easily manufactured, and has better mechanical strength and adhesion under thermal cycling. In this work, we focus on single layer coatings, but future work will include two layer systems.

As previously noted, the performance of the anti-reflective coating is dependent on the angle of the incoming light. Using equation 3.1 for non-normal incidence, reflection curves were plotted for use in selecting SLAR candidates; these curves for SiO₂ on Si and Ge substrates can be seen in Figure 4. The coating always improves the performance of the target bolometer. However, the improvement may not be sufficient to overcome the increased complexity and cost of adding the coating.

The above calculations assume all reflections are specular, the refractive index is constant throughout the thickness of the SLAR, and there are no losses in the SLAR ($k_{\text{SLAR}} = 0$). The incident light is also assumed to be unpolarized. This final assumption is not valid for TeO₂ due to birefringence. In this case, the refractive index varies between 1 and the true refractive index depending on the axis of propagation.

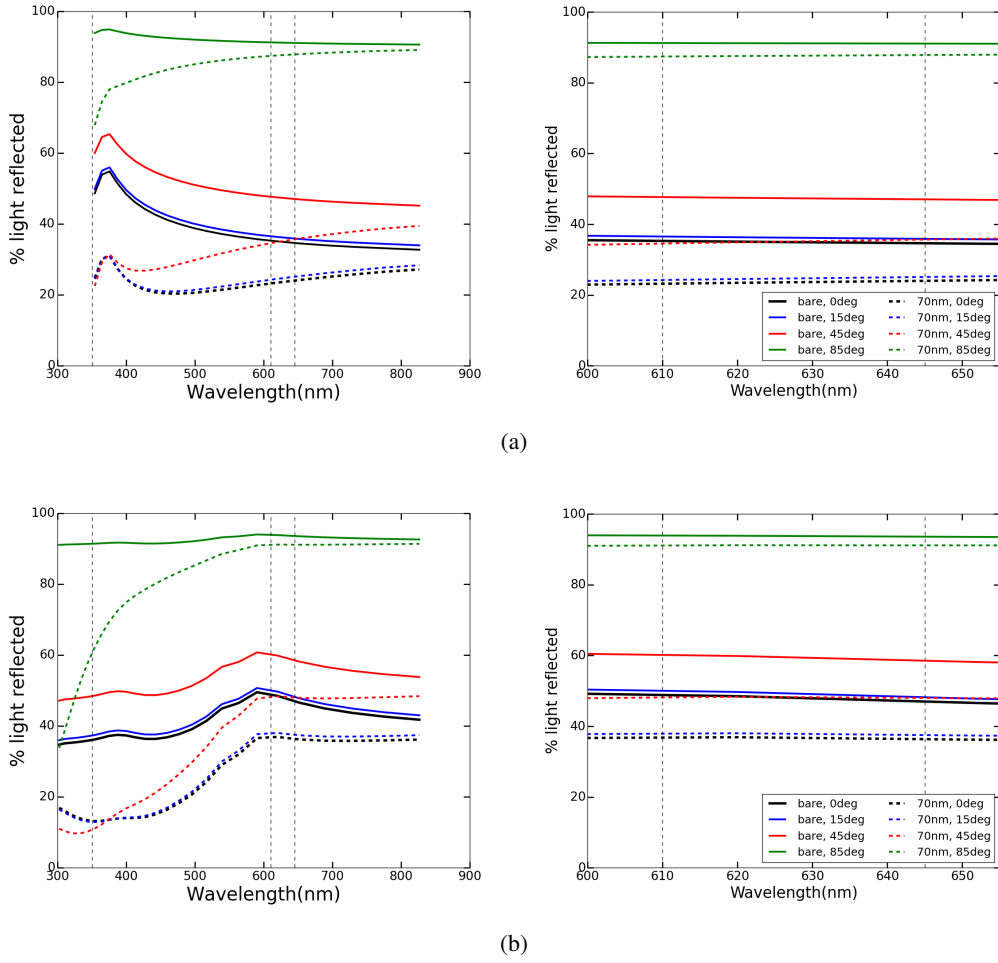


Figure 4. Dependence of reflection on angle of incidence for Si (a) and Ge (b). Values for bare substrate (solid) and 70 nm SiO₂ [25] single layer antireflective coating (dashed) are presented. Plots on left emphasize the wavelengths of interest (350 nm cutoff wavelength for TeO₂ and 610 nm and 645 nm scintillation peaks of ZnMoO₄ and ZnSe, respectively). Calculations are taken directly from equations 3.1-3.4 and contain no experimental data.

Based on their refractive index and availability, the following coatings were selected. For Ge, we study Al₂O₃, SiO₂, TiO₂, and HfO₂. For Si, we study SiO₂ and HfO₂. Figure 5 shows the wafers produced for this study. Al₂O₃ is a promising candidate. We were not able to obtain the materials to deposit it on Si, so it was only used for Ge.

4. Other Requirements

In addition to the target bolometer's optical properties, DM and $0\nu\beta\beta$ requirements have stringent requirements on surface and bulk radioactivity contamination for detector components. A complete background model like that constructed for CUORE[28] will set these specifications for the coating and substrate. The CUPID program already has extensive experience with the procurement and

Table 3. Characteristics of wafers used in this work

	Ge (1)	Ge (2)	Si
Orientation	crystalline, <100>	crystalline <100>	crystalline, <100>
Thickness	500 μm	350 μm	280 μm
Diameter	2 in	1 in	2 in
Doping	undoped	undoped	N Type, P Doped
Polish	2SP	1SP	1SP
Resistivity	>50 $\Omega\cdot\text{cm}$	30 $\Omega\cdot\text{cm}$	1-100 $\Omega\cdot\text{cm}$ (test)

handling of Ge and Si wafers. When the final candidate coating are chosen, the bulk material will need to be counted to ensure that it meets the desired specifications. Devoted tests will also be needed for understanding the coatings robustness under thermal cycling. This is all part of future work.

5. Fabrication

The 1-inch Ge wafers and 2-inch Si wafers were procured from University Wafer [29]. The 2 in Ge wafers were purchased from MTI Corporation [30]. Table 3 summarizes the properties of these wafers. The wafers were coated at the UCLA Nanoelectronics Research Facility (NRF) in a class-1000 multiuse cleanroom.

Al₂O₃, HfO₂, TiO₂ coatings Non-silicate coatings were deposited using a Fiji thermal atomic layer deposition (ALD) system. In such a system, precursors were pulsed into an Argon atmosphere such that for each pulse a single atomic layer adhered to the surface of the wafer. Each wafer was loaded into the machine at room temperature and atmosphere, and processed at 200 °C and 0.02 mTorr.

Al₂O₃ was used as a test wafer. It is a common coating that starts from TMA (trimethylaluminum) or Al(CH₃)₃. For HfO₂ coatings, precursors of Hf(NMe₂)₄ and H₂O were pulsed at 0.06 sec each until the desired thickness was reached. For TiO₂, coatings were processed similarly from a precursor of Tetrakis(Dimethylamido)Titanium (Ti(NMe₂)₄).

The ALD process was lengthy and required up to six hours to produce a single wafer. This technique has the advantage that more complex coating geometries can be achieved through nanopatterning. These geometries will be explored in future work.

SiO₂ coatings Silicate coatings were deposited using a High Deposition BMR plasma-enhanced chemical vapor deposition (PECVD). The system uses time-varying magnetic fields to generate highly dissociated plasmas of the precursor material which allows for a higher rate of deposition. Precursors of SiH₄ and O₂ gasses were used to create SiO₂ films at rates of up to 3000 Å/min. In the case of the BMR PECVD, the input is a desired time of deposition (as opposed to a desired thickness). This led to less precision in the final thickness of the coating; however, this process was very efficient and several wafers of different thicknesses could be produced over the course of a few hours.

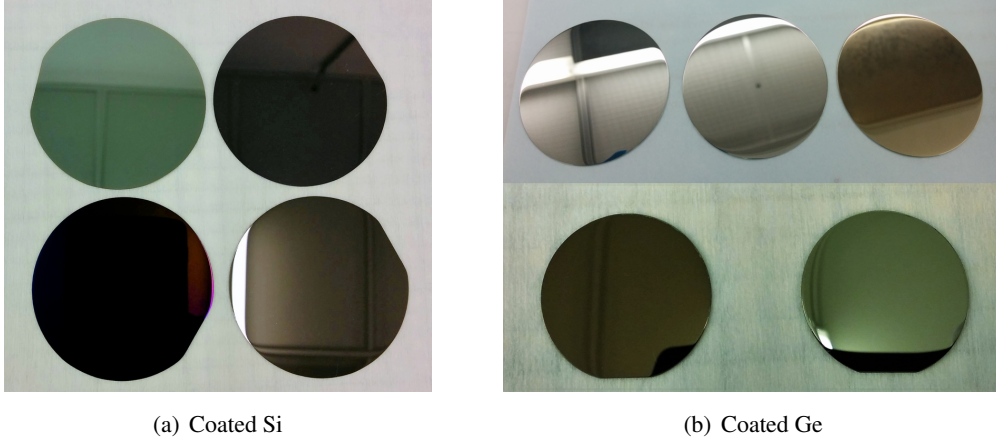


Figure 5. Wafers post-fabrication: (a) Si wafers clockwise from top left: SiO₂ 180 nm, SiO₂ 90 nm, SiO₂ 60 nm, HfO₂ 60 nm. (b) Ge wafers clockwise from top left: blank, Al₂O₃ 7 nm, TiO₂ 20 nm, SiO₂ 70 nm, TiO₂ 30 nm.

Table 4. Samples characterized for this study. Other samples were manufactured but their models did not reach acceptable goodness of fit values and therefore are not presented here. Discrepancies between ULVAC and Woolam measurements can be attributed to separate calibrations.

Sample #	Substrate	Coating	Thickness (nm) (ULVAC)	Thickness (nm) (Woolam)
1	Si	SiO ₂	66.116 ± 1.899	75.655 ± 0.021
2	Si	SiO ₂	79.627 ± 1.245	90.09 ± 0.49
3	Si	SiO ₂	181.902 ± 0.782	180.029 ± 0.037
4	Ge	SiO ₂	–	75.26 ± 2.294
5	Ge	SiO ₂	–	140.84 ± 3.13

6. Characterization

Samples were characterized using fixed and variable angle ellipsometry. The coated substrates were subjected to unpolarized light at an angle which reflected into a detector to measure the relative amplitude and phase of s- and p-polarizations. Relative amplitudes and phases of polarizations are described as a function of wavelength and angle by two variables [13]:

$$\tan \psi = \frac{|r_p|}{|r_s|} \quad \text{and} \quad \Delta = \delta_{rp} - \delta_{rs} \quad (6.1)$$

which can be combined to measure the total ratio of polarized reflections.

$$\tan \psi \exp(-i\Delta) = \frac{r_p(N_1, N_2, \theta_{inc}, d)}{r_s(N_1, N_2, \theta_{inc}, d)} \quad (6.2)$$

Figure 6 shows an example of representative Ψ/Δ data.

At this point, refractive index and thickness information for the coating was modeled and fit to experimental curves using equations 3.2-3.4. It was not possible to directly calculate total reflection

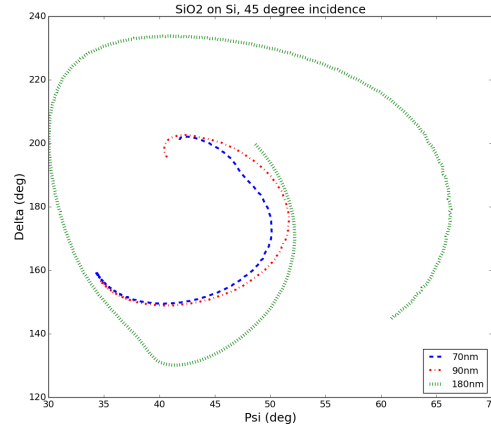


Figure 6. Example of ‘raw’ ellipsometric data Ψ and Δ (defined in Section 6). These values are then modeled using Cauchy film theory to find indexes of refraction shown in the next figure.

from these measurements, but a satisfactory result was found by reusing the calculated refractive index and thickness in equations 3.1-3.4. It should be noted that the measurement error of ψ and Δ are systematic; calculations of film thickness and optical characteristics are model dependent.

The UCLA Nanoelectronics Research Facility ULVAC UNECS-2000 fixed angle ellipsometer was used for immediate characterization of the Si wafers. Ge is less common, so no model was available. The UCSB Nanofabrication Facility’s Woollam M2000DI VASE Spectroscopic Ellipsometer was used to fully characterize all samples at variable angles.

Film thickness and single-point were analyzed in two groups. The ULVAC companion software was used for normal incidence, and the Woollam ellipsometer’s companion software *CompleteEase* was used for variable angle incidence. The results are shown in Table 4. SiO₂ coatings were assumed to follow Cauchy’s equation:

$$n(\lambda) = A + \frac{B}{\lambda^2} + \frac{C}{\lambda^4} + \dots \quad (6.3)$$

The resultant fits for SiO₂ on Si and Ge are shown in Figure 7. The goodness of fit of these curves is demonstrated by the root mean squared error, defined as:

$$\text{MSE} = \left[\frac{1}{3n - m} \sum_{i=1}^n \left\{ (N_{Ei} - N_{Gi})^2 + (C_{Ei} - C_{Gi})^2 + (S_{Ei} - S_{Gi})^2 \right\} \right]^{1/2} \cdot 1000 \quad (6.4)$$

where subscripts *E* and *G* refer to measured and modeled parameters, respectively, and

- n = number of wavelengths
- m = number of fit parameters = 3 (as follows)
- $N = \cos(2\Psi)$
- $C = \sin(2\Psi) \cos(\Delta)$
- $S = \sin(2\Psi) \sin(\Delta)$

The error in the parameters N , C and S that is introduced by the measurements is estimated to be typically 0.001, leading to the extra multiplicative factor of "1000". From equation 6.4, this implied that a fit with an MSE on the order of unity was considered in "perfect agreement" with the data. Values less than 100 were accepted for our purposes (as suggested by [31]). Fits for HfO_2 and TiO_2 samples had MSE values greater than 100, and were rejected. This method of testing goodness of fit is done automatically through the *CompleteEase* software. We found that non-standard coatings require specific calibrations of the ellipsometer. In the future, this will be done in order to characterize the total reflectivity and transmissivity of additional SLAR

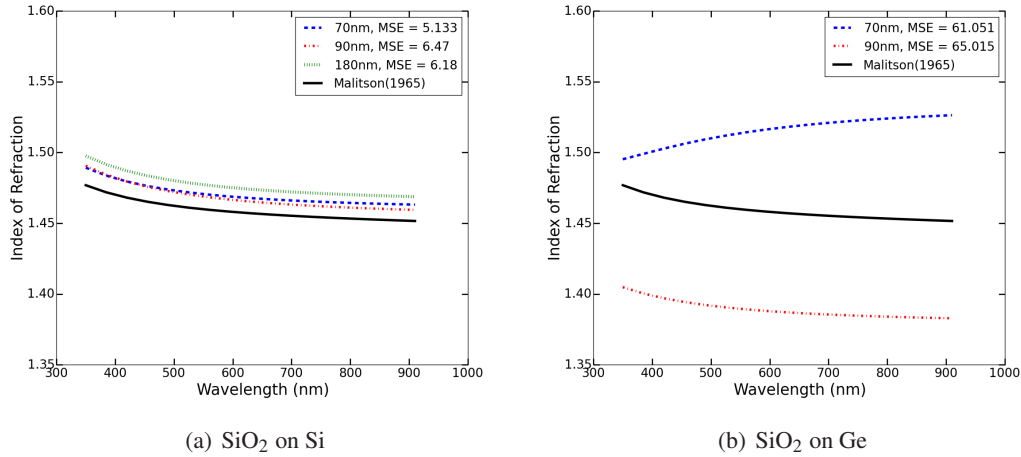


Figure 7. Refractive index fit for SiO_2 on (a) Si and (b) Ge. MSE values correspond to goodness of fit (see Eq 6.4; $\text{MSE} < 10$ are excellent, $\text{MSE} < 100$ are acceptable). Black solid line indicates literature values.

7. Predicted Reflectance

From the indexes characterized in Figure 7, it is possible to reproduce the reflectivity curves for each system. The indices are used as input to equations 3.1-3.4 and plotted for various thicknesses and angles of incidence¹; the results for Si are shown in Figure 8; the results for Ge are shown in Figure 9. All curves are plotted in reference to the reflectance for a bare substrate at normal incidence, and the calculation assumes all reflections are specular and there are no losses in the SLAR ($k_{\text{SLAR}} = 0$).

For the peak scintillation wavelengths, 645 nm and 610 nm for ZnSe and ZnMoO_4 , it is clear that Si substrate reflectivity can be improved with any of the tested SLAR thicknesses: at normal incidence, a 90 nm coating of SiO_2 improves reflectivity of an Si substrate by $\sim 25\%$. The performance of the system depends heavily on the film thickness: 180 nm films do not show nearly the same decrease in reflectivity except at higher angles; see Figure 8. In contrast, the Ge substrate performance does not depend as heavily on the SLAR thickness. Improvements of up to 22% were seen for normal incidence for both 75 nm and 140 nm SiO_2 coatings on Ge. For the scintillation

¹Incident angles are plotted up to the ellipsometer maximum of 85° , although calculations suggest the true maximum could be larger.

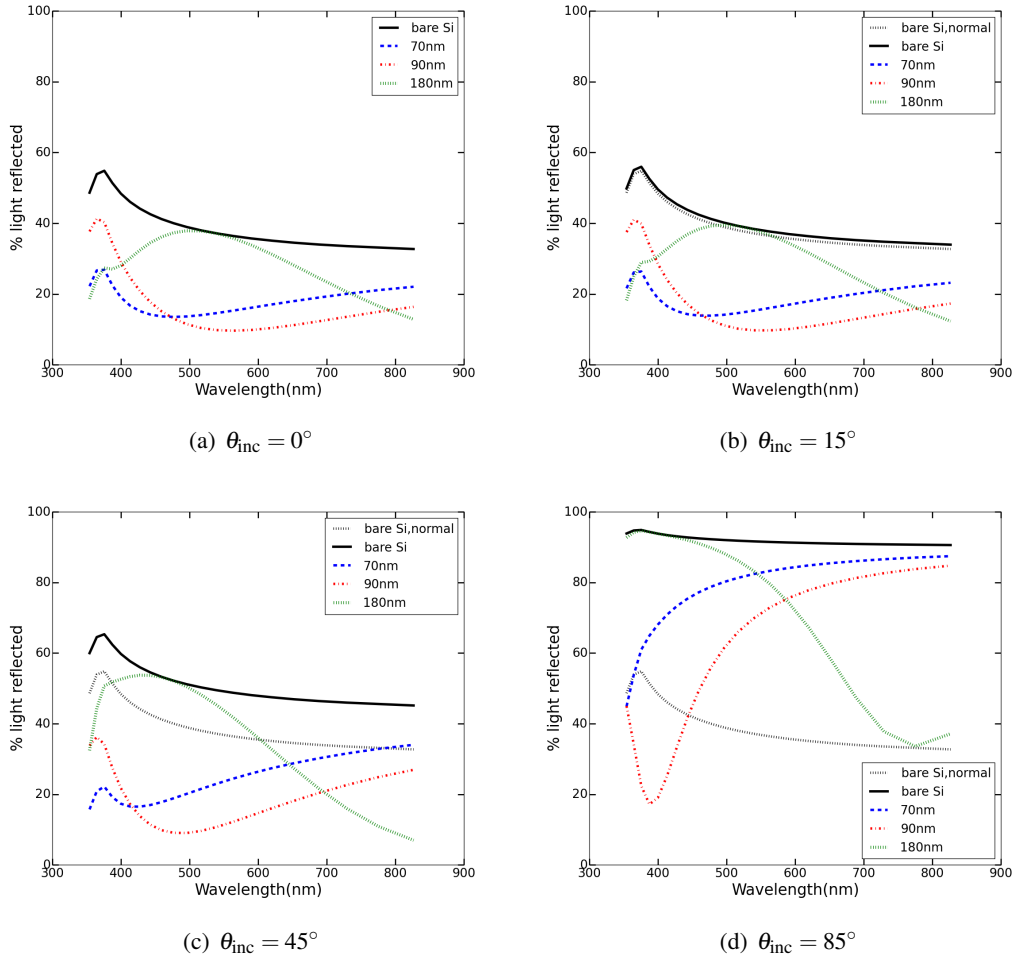


Figure 8. Predicted reflectivity values for SiO₂ coating on Si substrate for varied angles of incidence. Black solid curve indicates reflectivity of bare Si [6]. Angles of incidence are as follows: (a) 0°, (b) 15°, (c) 45°, (d) 85°. Colored reflectivity curves are calculated based on ellipsometric measurements for $n(\lambda)$ (see Figure 7). Thicknesses of 70, 90, and 180 nm (with MSE values 5.13, 6.47 and 6.18 respectively) are displayed. For plots (b)-(d), the reflectivity curve for normal incidence is provided as a reference (black dotted). For all angles of incidence and thicknesses, coating with SiO₂ should improve reflectivity. Recommendations for wavelengths of interest can be found in Section 7.

wavelength of ZnSe (645 nm), the predicted improvement is $\sim 20\%$, which agrees with the findings of previous work [32].

For a signal from Cherenkov light, the solution is quite different. TeO₂ has a cutoff wavelength at 350 nm. At this wavelength, it is difficult for a Si substrate to get below 20% reflectivity, so a Ge substrate is a better choice. These results indicate a Ge substrate with a 70 nm SiO₂ coating is better than larger thicknesses.

As seen in Figures 8 and 9, results also demonstrate that the performance of these light-collecting, target bolometers is greatly affected by the angle of incident light. Significant amounts of light will be lost simply due to reflectivity: scintillation light incident on Ge from a ZnMoO₄

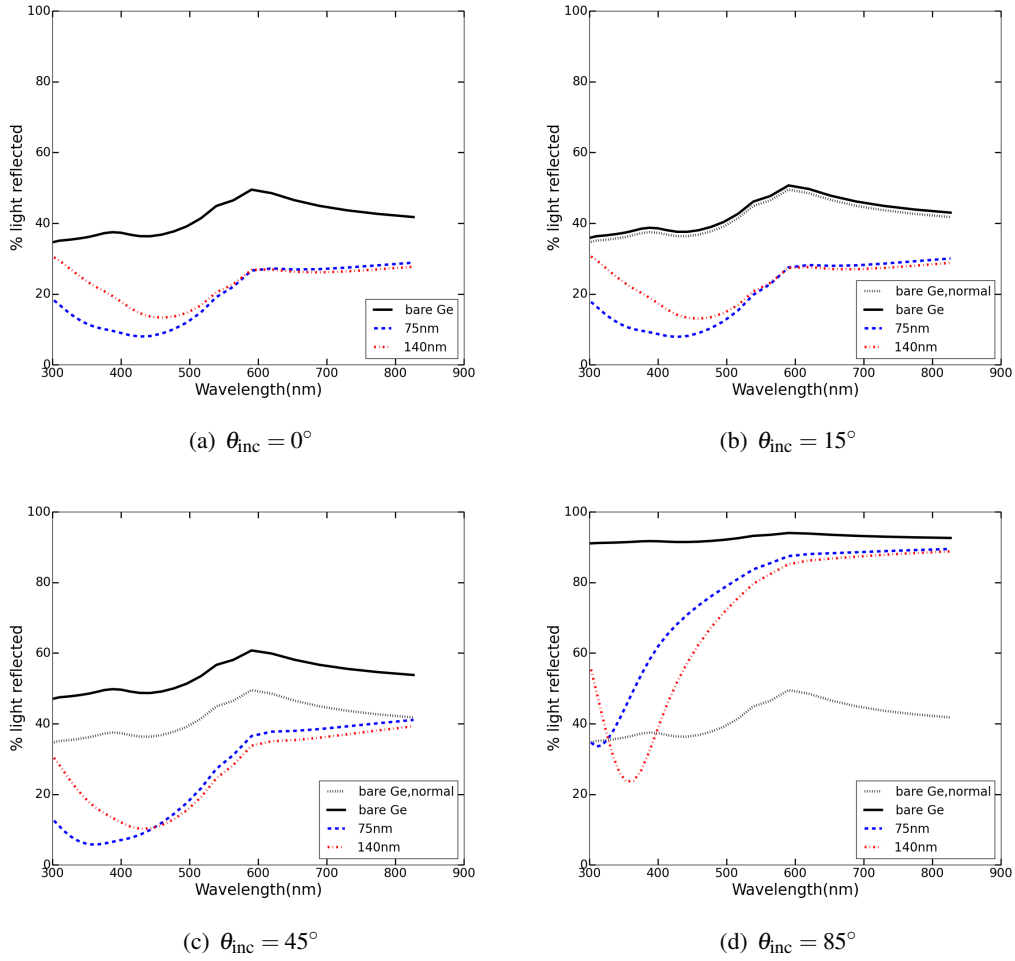


Figure 9. Predicted reflectivity values for SiO₂ coating on Ge substrate for varied angles of incidence. Black solid curve indicates reflectivity of bare Si [6]. Angles of incidence are as follows: (a) 0°, (b) 15°, (c) 45°, (d) 85°. Colored reflectivity curves are calculated based on ellipsometric measurements for $n(\lambda)$ (see Figure 7). Thicknesses of 75 and 140 nm (with MSE values 61.05 and 65.02 respectively) are displayed. For plots (b)-(d), the reflectivity curve for normal incidence is provided as a reference (black dotted). For all angles of incidence and thicknesses, coating with SiO₂ should improve reflectivity. Recommendations for wavelengths of interest can be found in Section 7.

primary bolometer at 45° (in the plane of incidence) will be reflected at a 65% loss (see Figure 9(c)). An antireflective coating of 140nm SiO₂ can decrease this loss to only about 35%.

8. Conclusion

Anti-reflective coatings can significantly increase the efficiency of light collection bolometers in rare event searches with the purpose of reducing background rates. Several coatings were manufactured successfully on Ge and Si substrates and characterized at room temperature using variable angle ellipsometry. Full characterization of the more rare HfO₂ and TiO₂ coatings was unsuccessful.

ful. Preliminary calculations for both Si and Ge substrates confirm a decrease in reflectivity from SiO₂ coatings of various thicknesses at various angles of incidence, an improvement on the calculations performed by [32] which assumed normal incidence. For the ZnSe and ZnMoO₄ scintillation wavelengths of 645 nm and 610 nm, coatings of 90 nm SiO₂ on Si or 140 nm SiO₂ on Ge are recommended. For Cherenkov light from TeO₂ at 350 nm, a Ge substrate with a 70 nm SiO₂ coating is recommended. Work is ongoing to fully characterize all coatings at operating and room temperatures, as well as to explore the potential of novel coating techniques. Additional analysis of the impact of the coatings on system radiopurity and testing of the coatings characteristic bolometric operating temperatures will fully establish the value of SLAR coatings in rare event searches.

Acknowledgments

This work was funded by the Hellman Fellow program at UCLA. Special thanks to the UCLA NanoLab (Max Ho, Tom Lee, Wilson Lin) and UCSB NanoLab (Tom Reynolds, Brian Thibeault). Many thanks also to Matteo Biassoni, Huan Huang, Jacob Feintzeig, Laura Gladstone, Jon Ouellet, and other CUORE collaborators for their valuable insight and discussion. A special thank you to Laura Gladstone and Jacob Siegel for editing the manuscript.

References

- [1] The CUPID Interest Group, *CUPID: CUORE (Cryogenic Underground Observatory for Rare Events) Upgrade with Particle Identification*, 2015.
- [2] G. Angloher, A. Bento, C. Bucci, L. Canonica, X. Defay, A. Erb, F. von Feilitzsch, N. F. Iachellini, P. Gorla, A. Gütlein, D. Hauff, J. Jochum, M. Kiefer, H. Kluck, H. Kraus, J. C. Lanfranchi, J. Loebell, A. Münster, C. Pagliarone, F. Petricca, W. Potzel, F. Pröbst, F. Reindl, K. Schäffner, J. Schieck, S. Schönert, W. Seidel, L. Stodolsky, C. Strandhagen, R. Strauss, A. Tanzke, H. H. Trinh Thi, C. Türkoğlu, M. Uffinger, A. Ulrich, I. Usherov, S. Wawoczny, M. Willers, M. Wüstrich, and A. Zöller, *Results on light dark matter particles with a low-threshold CRESST-II detector*, *The European Physical Journal C* **76** (1, 2016) 25.
- [3] M. Kiefer, G. Angloher, A. Bento, C. Bucci, L. Canonica, A. Erb, F. Feilitzsch, N. Ferreiro Iachellini, P. Gorla, A. Gütlein, D. Hauff, J. Jochum, H. Kluck, H. Kraus, J.-C. Lanfranchi, J. Loebell, A. Münster, F. Petricca, W. Potzel, F. Pröbst, F. Reindl, S. Roth, K. Rottler, C. Sailer, K. Schäffner, J. Schieck, S. Schönert, W. Seidel, M. Sivers, L. Stodolsky, C. Strandhagen, R. Strauss, A. Tanzke, C. Türkoğlu, M. Uffinger, A. Ulrich, I. Usherov, S. Wawoczny, M. Willers, M. Wüstrich, and A. Zöller, *In-situ study of light production and transport in phonon/light detector modules for dark matter search*, *Nuclear Instruments and Methods in Physics Research Section A: Accelerators, Spectrometers, Detectors and Associated Equipment* **821** (2016) 116–121.
- [4] V. U. o. O. Mikhailik and H. U. o. O. Kraus, *Performance of scintillation materials at cryogenic temperatures*, 2010.
- [5] S. K. J. Al-Ani, C. A. Hogarth, and R. A. El-Malawany, *A study of optical absorption in tellurite and tungsten-tellurite glasses*, *Journal of Materials Science* **20** no. 2 661–667.
- [6] D. E. Aspnes and A. A. Studna, *Dielectric functions and optical parameters of Si, Ge, GaP, GaAs, GaSb, InP, InAs, and InSb from 1.5 to 6.0 eV*, *Physical Review B* **27** (1983), no. 2 985–1009.
- [7] **GEANT4** Collaboration, S. Agostinelli et al., *GEANT4: A Simulation toolkit*, *Nucl. Instrum. Meth.* **A506** (2003) 250–303.

- [8] J. Allison et al., *Geant4 developments and applications*, *IEEE Trans. Nucl. Sci.* **53** (2006) 270.
- [9] J. Allison, K. Amako, J. Apostolakis, P. Arce, M. Asai, T. Aso, E. Bagli, A. Bagulya, S. Banerjee, G. Barrand, B. Beck, A. Bogdanov, D. Brandt, J. Brown, H. Burkhardt, P. Canal, D. Cano-Ott, S. Chauvie, K. Cho, G. Cirrone, G. Cooperman, M. Cortázar-Giraldo, G. Cosmo, G. Cuttone, G. Depaola, L. Desorgher, X. Dong, A. Dotti, V. Elvira, G. Folger, Z. Francis, A. Galoyan, L. Garnier, M. Gayer, K. Genser, V. Grichine, S. Guatelli, P. Guàrdia, P. Gumplinger, A. Howard, I. Hârlău, I. Ivnič, L. Žitňák, S. Hwang, S. Incerti, A. Ivanchenko, V. Ivanchenko, F. Jones, S. Jun, P. Kaitaniemi, N. Karakatsanis, M. Karamitros, M. Kelsey, A. Kimura, T. Koi, H. Kurashige, A. Lechner, S. Lee, F. Longo, M. Maire, D. Mancusi, A. Mantero, E. Mendoza, B. Morgan, K. Murakami, T. Nikitina, L. Pandola, P. Paprocki, J. Perl, I. Petrović, M. Pia, W. Pokorski, J. Quesada, M. Raine, M. Reis, A. Ribon, A. R. Fira, F. Romano, G. Russo, G. Santin, T. Sasaki, D. Sawkey, J. Shin, I. Strakovsky, A. Taborda, S. Tanaka, B. Tomášek, T. Toshito, H. Tran, P. Truscott, L. Urban, V. Uzhinsky, J. Verbeke, M. Verderi, B. Wendt, H. Wenzel, D. Wright, D. Wright, T. Yamashita, J. Yarba, and H. Yoshida, *Recent developments in geant4, Nuclear Instruments and Methods in Physics Research Section A: Accelerators, Spectrometers, Detectors and Associated Equipment* **835** (2016) 186 – 225.
- [10] L. Bergé and E. al., *Purification of molybdenum, growth and characterization of medium volume ZnMoO₄ crystals for the LUMINEU program*, *Journal of Instrumentation* **9** (2014), no. 06 P06004.
- [11] J. Beeman and E. al., *ZnMoO₄: A promising bolometer for neutrinoless double beta decay searches*, *Astroparticle Physics* **35** (2012), no. 12 813–820.
- [12] M. Green, *Self-consistent optical parameters of intrinsic silicon at 300 K including temperature coefficientss*, *Solar Energy Materials and Solar Cells* **92** (2008), no. 11 1305–1310.
- [13] H. G. Tompkins, *A User's Guide to Ellipsometry*. Academic Press, In., San Diego, CA, 1993.
- [14] J. Connolly, B. DiBenedetto, and R. Donadio, *Specifications Of Raytran Material*, in *Proc. SPIE*, vol. 0181, pp. 141–144, SPIE, 1979.
- [15] D. M. Chernyak, F. A. Danevich, V. Y. Degoda, I. M. Dmitruk, F. Ferri, and E. N. Galashov, *Nuclear Instruments and Methods in Physics Research A Optical , luminescence and thermal properties of radiopure ZnMoO₄ crystals used in scintillating bolometers for double beta decay search*, *Nuclear Inst. and Methods in Physics Research, A* **729** (2013) 856–863.
- [16] N. Uchida, *Optical properties of single-crystal paratellurite (TeO₂)*, *Physical Review B* **4** (1971), no. 10 3736–3745.
- [17] M. Mancuso, J. Beeman, a. Giuliani, L. Dumoulin, E. Olivieri, G. Pessina, O. Plantevin, C. Rusconi, and M. Tenconi, *An experimental study of antireflective coatings in Ge light detectors for scintillating bolometers*, *EPJ Web of Conferences* **65** (1, 2014) 04003.
- [18] W. Dash and R. Newman, *Intrinsic Optical Absorptionin Single-Crystal Germanium and Silicon at 77K and 300K*, *Physical Review* **99** (1955), no. 4.
- [19] A. Rahman, A. Ashraf, H. Xin, X. Tong, P. Sutter, M. D. Eisaman, and C. T. Black, *Sub-50-nm self-assembled nanotextures for enhanced broadband antireflection in silicon solar cells*, *Nature Communications* **6** (2015) 5963.
- [20] N. Coron, P. de Marcillac, J. Leblanc, G. Dambier, and J. P. Moalic, *Highly sensitive large-area bolometers for scintillation studies below 100 mK*, *Optical Engineering* **43** (2004) 1568–1576.

- [21] M. Biassoni, C. Brofferio, S. Capelli, L. Cassina, M. Clemenza, O. Cremonesi, M. Faverzani, E. Ferri, A. Giachero, L. Gironi, C. Giordano, C. Gotti, M. Maino, B. Margesin, A. Nucciotti, M. Pavan, G. Pessina, E. Previtali, A. Puiu, M. Sisti, and F. Terranova, *Large area Si low-temperature light detectors with Neganov-Luke effect*, .
- [22] I. H. Malitson and M. J. Dodge, *Refractive Index and Birefringence of Synthetic Sapphire*, in *J. Opt. Soc. Am.*, no. 62, p. 1405, 1972.
- [23] D. L. Wood, K. Nassau, T. Y. Kometani, and D. L. Nash, *Optical properties of cubic hafnia stabilized with yttria*, *Applied optics* **29** (1990), no. 4 604–607.
- [24] H. R. Philipp, *Optical Properties of Silicon Nitride*, *Journal of The Electrochemical Society* **120** (1973), no. 2 295.
- [25] L. Gao, R. Lemarchand, and M. Lequime, *Refractive index determination of SiO₂ layer in the UV/Vis/NIR range: Spectrophotometric reverse engineering on single and bi-layer designs*, *Journal of the European Optical Society* **8** (2013) 13010–1.
- [26] J. R. Devore, *Refractive Indices of Rutile and Sphalerite*, *Journal of the Optical Society of America* **41** (1951), no. 6 416.
- [27] J. W. Fleming, *Dispersion in GeO₂ SiO₂ glasses*, *Applied Optics* **23** (1984), no. 24 4486–4493.
- [28] **CUORE** Collaboration, C. Alduino et al., *The projected background for the CUORE experiment*, *Submitted to: Eur. Phys. J. C* (2017) [arXiv:1704.0897].
- [29] “<http://www.universitywafer.com/>.”
- [30] “<http://www.mtixtl.com/>.”
- [31] J. A. Woollam Co. Inc, *CompleteEASE Data Analysis Manual*, 2008.
- [32] J. W. Beeman, F. Bellini, P. Benetti, L. Cardani, N. Casali, D. Chiesa, M. Clemenza, I. Dafinei, S. Di Domizio, F. Ferroni, A. Giachero, L. Gironi, A. Giuliani, C. Gotti, M. Maino, S. Nagorny, S. Nisi, C. Nones, F. Orio, L. Pattavina, G. Pessina, G. Piperno, S. Pirro, E. Previtali, C. Rusconi, M. Tenconi, C. Tomei, and M. Vignati, *Current Status and Future Perspectives of the LUCIFER Experiment*, *Advances in High Energy Physics* **2013** (2013) 1–15.